Supplement of Atmos. Chem. Phys., 25, 14435–14448, 2025
https://doi.org/10.5194/acp-25-14435-2025-supplement

Atmospheric Chemistry and Physics
Open Access
EGU

Supplement of

The historical climate trend resulted in changed vertical transport patterns in climate model simulations

Adrienne Jeske and Holger Tost

Correspondence to: Adrienne Jeske (adjeske@uni-mainz.de)

S1 Modifications to CVTRANS

S1.1 Adaptation of the closure

Following Tiedtke (1989), the detrainment and the entrainment are given by an organised and a turbulent driven component. This is equally valid for the downdraft and the updraft. In the Tiedtke-Nordeng scheme, the same approach is made (Nordeng, 1994).

In the former versions of CVTRANS by Tost et al. (2010) and Ouwersloot et al. (2015), it could happen in some cases that the formulation of the closure eliminated the turbulent entrainment and detrainment. To fulfil Eq. (1a) and (1b), it could occur that the entrainment had to be set to zero to close the mass balance. However, this would also erroneously eliminate the turbulent entrainment, which is always active in rapidly ascending or descending air masses. The entrainment rate is given by

$$E_{\mathrm{u}}^{k} = F_{\mathrm{u}}^{k} - F_{\mathrm{u}}^{k+1} + D_{\mathrm{u}}^{k}, \tag{S1}$$

as long as the updraft mass flux leaving the box at its top is larger than the incoming updraft mass flux from below. All quantities are positive by definition.
If the incoming updraft mass flux is larger than the mass flux leaving the box at the top, the detrainment will be recalculated with the help of the closure as follows

$$D_{\mathrm{u}}^{k} = F_{\mathrm{u}}^{k+1} - F_{\mathrm{u}}^{k} + E_{\mathrm{u}}^{k}. \tag{S2}$$

If both equations for entrainment and detrainment are properly solved, the detrainment or entrainment will not be accidentally set to zero. The same approach is taken for the downdraft.

As turbulent mixing is always present according to Tiedtke (1989), the existence of a minimal turbulent entrainment and detrainment is ensured and the closure corrects potentially erroneous zero turbulent events.
The adaptive time stepping by Ouwersloot et al. (2015) must be applied. Otherwise, the calculation of the air mass transport can lead to negative values or a reduction of the strength of the mass fluxes.

S1.2 Detrainment of entrained air in the downdraft

In CVTRANS, the parameter f_{det} gives the portion of material that is detrained directly after the entrainment in the same box as described by Ouwersloot et al. (2015). f_{det} is only computed and applied for the calculations concerning the updraft detrainment. Taking turbulence into account, we need to adapt Eq. (2) from Ouwersloot et al. (2015) also for the downdraft:

$$C_{\mathrm{d,det}}^{k} = \frac{(D_{\mathrm{d}}^{k} - f_{\mathrm{det}} E_{\mathrm{d}}^{k}) C_{\mathrm{d}}^{k} + f_{\mathrm{det}} E_{\mathrm{d}}^{k} C_{\mathrm{env}}^{k}}{D_{\mathrm{d}}^{k}}. \tag{S3}$$

Thereby, C denotes the concentration of a tracer.

S2 Example of a convective exchange matrix for one specific event

Figure S1(b) shows the convective exchange matrix for a snapshot of a deep convective event over continental Western Australia in austral summer. The levels of origin are given on the horizontal axes (where the air comes from), and the vertical axes denote the destination level (where the air is transported to). The model levels are shown alongside the corresponding pressure levels. Level 31 is closest to the surface and is associated with a pressure of 938 hPa. The main diagonal is strongly pronounced, indicating that a great portion is not affected by the convection. About 34% of the air mass stays at least within its origin level. The diagonals at higher destination pressures than the main diagonal show the impact of the mass-balancing subsidence. Up to 38% of the air mass is descending from its origin level directly to the level below. In the mid troposphere, the mass portion in the diagonal closest to the main diagonal is higher than the one in the main diagonal. The diagonals closer to the surface have much smaller values, i.e., in those levels the mass balancing subsidence is weaker, as also usually the updrafts below the cloud base are weaker than within the cloud.

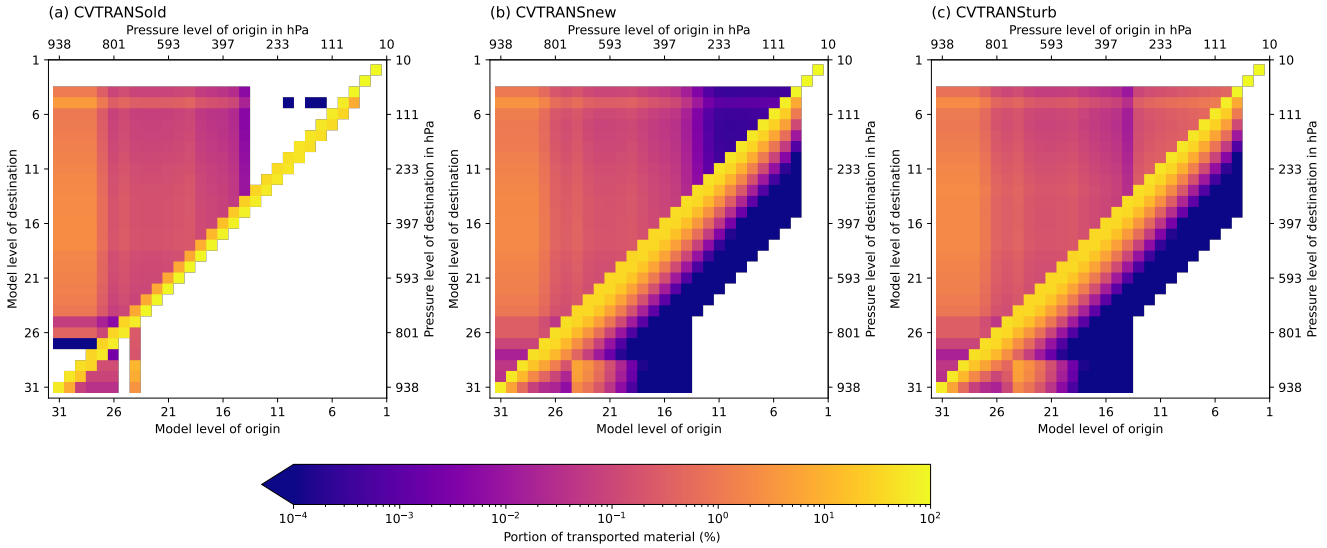

Figure S1: Convective exchange matrix for one snapshot of one specific event. The convective event was located over Western Australia in the austral summer (23.316°S, 120.000°E on 1st January 1979 at 5 UTC). The convective exchange matrix is displayed for one time step. (a) shows the convective exchange matrix calculated with CVTRANSold, (b) the convective exchange matrix calculated with CVTRANS v3.0 (CVTRANSnew), and (c) the convective exchange matrix as (b) but with enhanced turbulent mixing (CVTRANSturb).

The downdraft is visible in the lower left corner of Fig. S1(b). At 719 hPa (level 24), the impact of the downdraft is strongest. Starting at 719 hPa, nearly 6% of the air mass is transported to 873 hPa (level 28) and close to 5% to 903 hPa (level 29). The downdraft and the subsidence partially overlap. The transport effect by subsidence becomes weaker with larger vertical distances (the more levels are overcome). The transport from level 719 hPa to 839 hPa (level 27) is weaker than the transport to 873 hPa (level 26). Therefore, the mass transport to 873 hPa can be mainly attributed to the downdraft.

The deep upward transport reaches up to 90 hPa. The main outflow level is located at 111 hPa. That can be seen by the lighter colours in the upper part of Fig. S1(b) compared to the darker colours of the other destination levels. About 3% originating at 938 hPa to 873 hPa (level 31 to 28) reaches the main outflow level. Less than 1% of the air mass from starting at 801 hPa (level 26) and levels with lower pressures is transported upward to 90 hPa. These seem to be rather small portions; however, only 69% of the original air mass stays within the main outflow level. This highlights the impact of convection on the atmospheric composition.

Figure S1(a) shows the convective exchange matrix for the same event as (b) but with using the old CVTRANS (CVTRANSold) and without applying adaptive time stepping. The latter leads to only one diagonal below the main diagonal as the subsidence can not reach further than one model level. The "missing values" in the lower left and upper right part of the convective exchange matrix (Fig. S1(a)) is related to the incorrectly missing turbulent entrainment and turbulent detrainment which is fixed in CVTRANS v3.0 as described in Sec. S1. If turbulent mixing is considered as strong as suggested by Tiedtke (1989), the convective exchange matrix is given by Fig. S1(c). This leads to a largely reduced direct upward transport from the boundary layer to the upper troposphere, which does not match observations. CVTRANS v3.0 is physically more consistent than CVTRANSold but does not deviate from CVTRANSold as hugely as CVTRANSturb in terms of the intrusion of boundary layer air into the upper troposphere.

S3 EMAC Submodels

Table S1: Used submodels.

Submodel	Reference
SWITCH	Jöckel et al. (2005)
CHANNEL	Jöckel et al. (2010)
TRACER	Jöckel et al. (2008)
TIMER	Jöckel et al. (2010)
QTIMER	Jöckel et al. (2010)
IMPORT	Kerkweg and Jöckel (2015)
GRID	Kerkweg et al. (2018)
RND	Jöckel et al. (2010)
TENDENCY	Eichinger and Jöckel (2014)
AEROPT	Dietmüller et al. (2016)
ALBEDO	Nützel et al. (2024)
CH4	Winterstein and Jöckel (2021)
CLOUD	Lohmann and Roeckner (1996)
CLOUDOPT	Dietmüller et al. (2016)
CONVECT	Tost et al. (2006)
CVTRANS	Tost et al. (2010)
JVAL	Sander et al. (2014), Landgraf and Crutzen (1998)
ORBIT	Dietmüller et al. (2016)
PTRAC	Jöckel et al. (2008)
QBO	Jöckel et al. (2006), Giorgetta and Bengtsson (1999)
RAD	Dietmüller et al. (2016)
E5VDIFF	Roeckner et al. (2006)
SURFACE	Roeckner et al. (2006), Hagemann (2002)
TNUDGE	Kerkweg et al. (2006)
TROPOP	Jöckel et al. (2006)
VISO	Jöckel et al. (2010)

S4 Corresponding reference values for the tropopause height and the boundary layer height

Table S2: Reference values for the tropopause and the boundary layer height. In this table information is provided which model and approximate pressure levels correspond to the simulated tropopause. Additionally, the approximate reference model level and heights in meters are shown for the boundary layer height. In this study, we relate the tropics to the area between 30°N and 30°S and the extra-tropics to the area between 30°N/S and 60°N/S. We do not claim that this table is exact nor includes all possible model levels, pressures and heights of the tropopause and the boundary layer. The given values should be considered as rough guidance only.

Reference	Model level tropics	Pressure tropics	Model level extra-tropics	Pressure extra-tropics
Tropopause	15 to 4	340 to 60 hPa (130 to 100 hPa)	19 to 6	410 to 110 hPa (390 to 170 hPa)
Reference	Model level tropics	Height tropics	Model level extra-tropics	Height extra-tropics
Boundary layer	31 to 22	0 to 3000 m	31 to 19	0 to 4400 m

S5 Convective exchange matrix changes from 1990 to 1999 and from 2000 to 2009 compared with 1980 to 1989

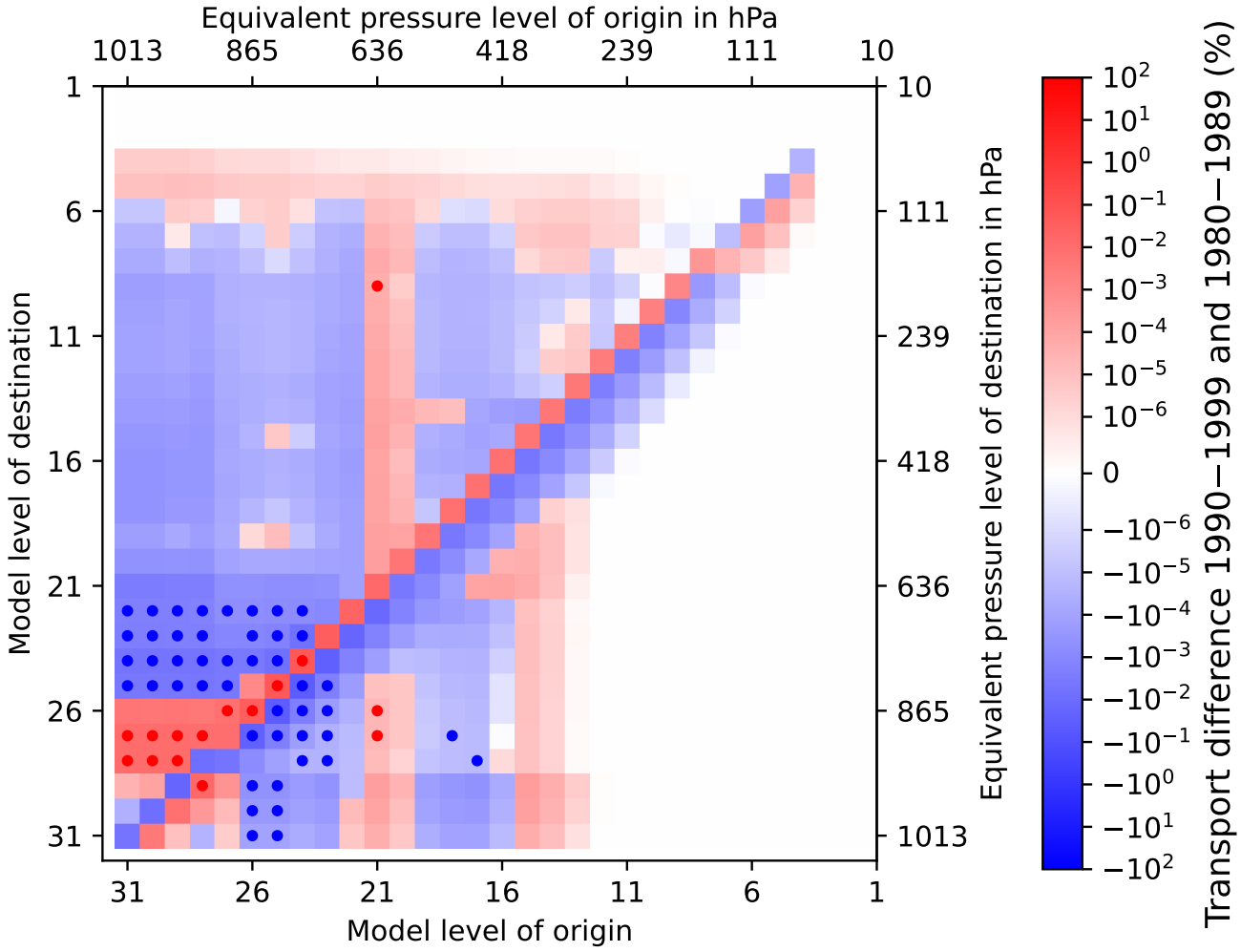

Figure S2: Changes in the convective mean transport between 60°S and 60°N. The difference is shown between the temporal (ten year) and global (area weighted) convective exchange matrix form 1990 to 1999 and the one from 1980 to 1989. Red colours denote that the values were higher in the period 1990 to 1999 and blue boxes show that the entry in the convective exchange matrix was higher from 1980 to 1989. A dot in a box indicates statistical significance. A two sided student t-test was used with a significance threshold of 1% for every side of the t-distribution.

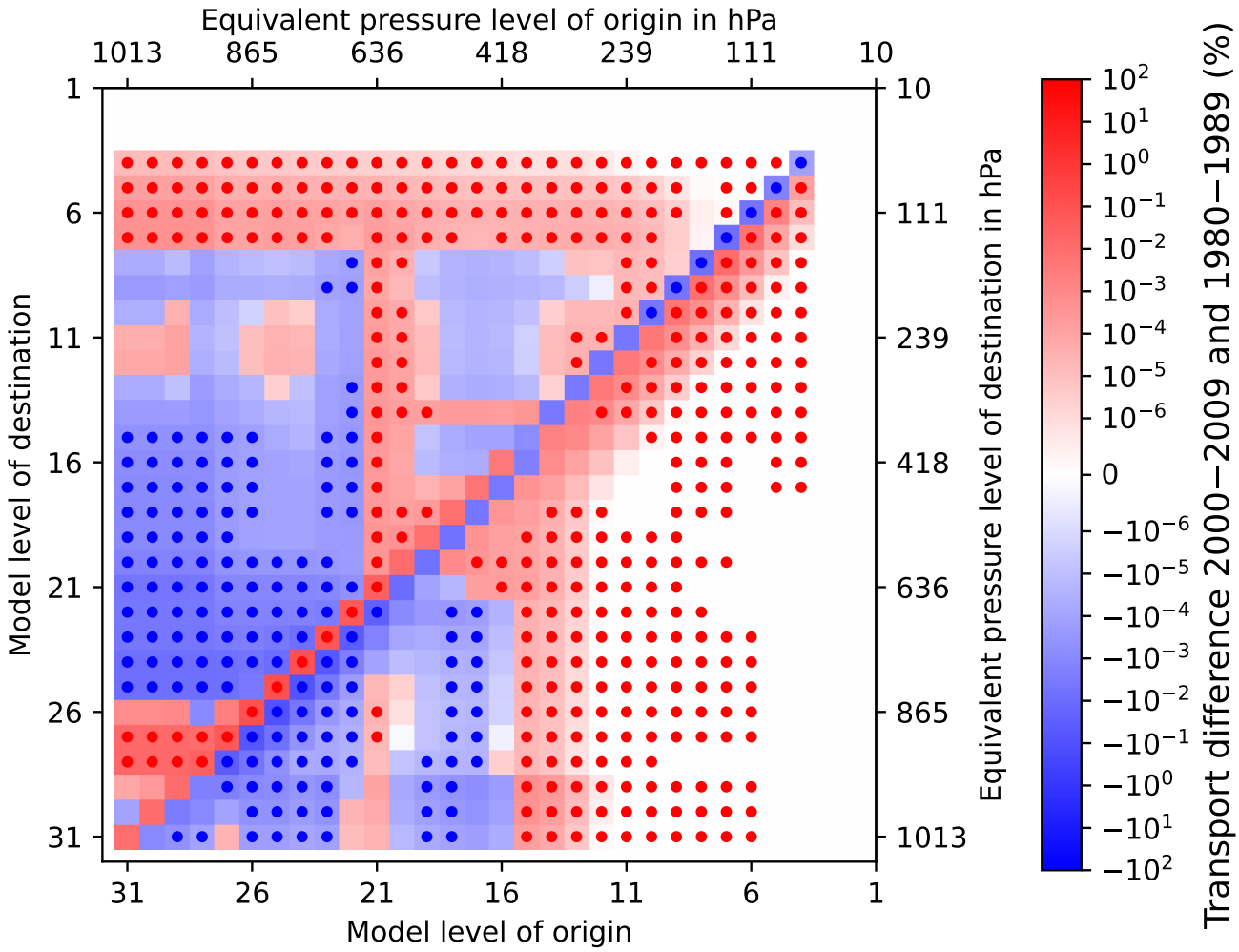

Figure S3: Changes in the convective mean transport between 60°S and 60°N. The difference is shown between the temporal (ten year) and global (area weighted) convective exchange matrix form 2000 to 2009 and the one from 1980 to 1989. Red colours denote that the values were higher in the period 2000 to 2009 and blue boxes show that the entry in the convective exchange matrix was higher from 1980 to 1989. A dot in a box indicates statistical significance. A two sided student t-test was used with a significance threshold of 1% for every side of the t-distribution.

S6 El Niño and La Niña

The La Niña event (Fig. S4) has similar patterns as the ten year mean. That was to be expected because La Niña is characterised by a strongly pronounced Walker circulation. In contrast, the direction of the circulation changes in the El Niño case leading to changes in the convective transport patterns (Fig. S5). These are especially large over the central Pacific. In the La Niña case, almost no deep convective transport was active at the equator in the considered time period. In contrast, BL to UT transport is specifically pronounced during the El Niño event in exactly this region.

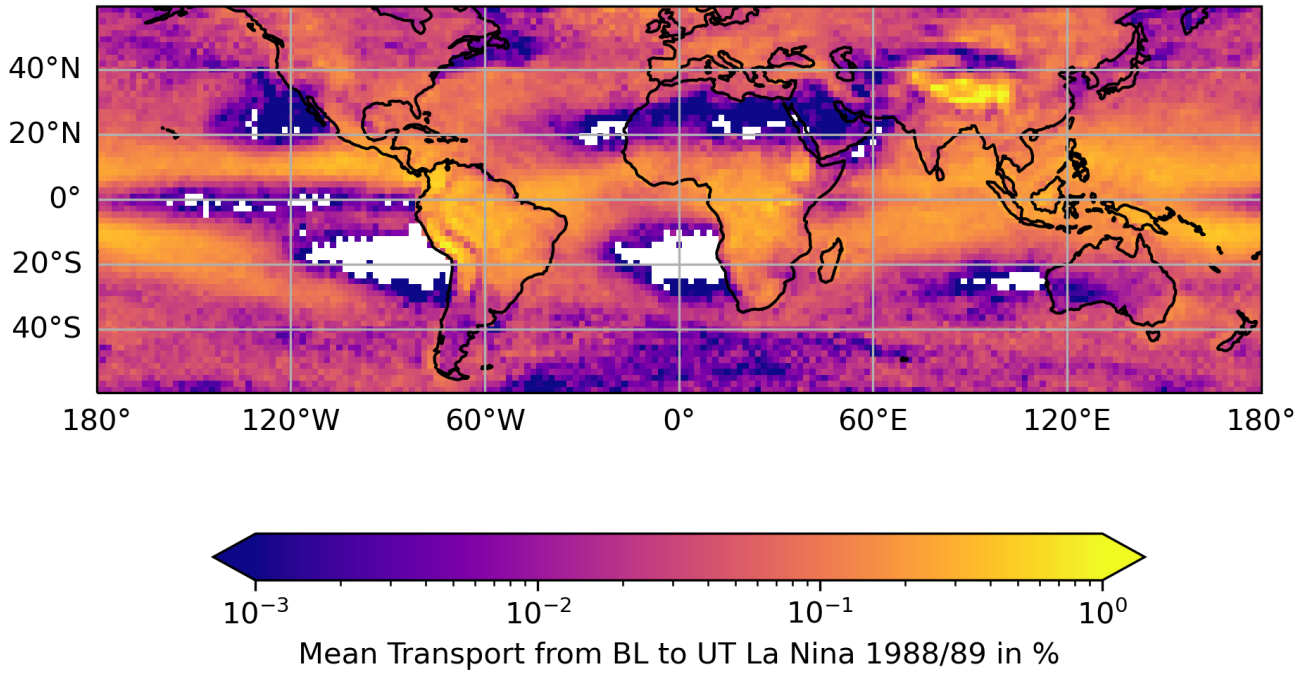

Figure S4: La Niña event 1988/89 convective mean transport from the planetary boundary layer height to upper troposphere within 12 min. The upper troposphere is defined as the region between the tropopause and the pressure height of tropopause plus 150 hPa.

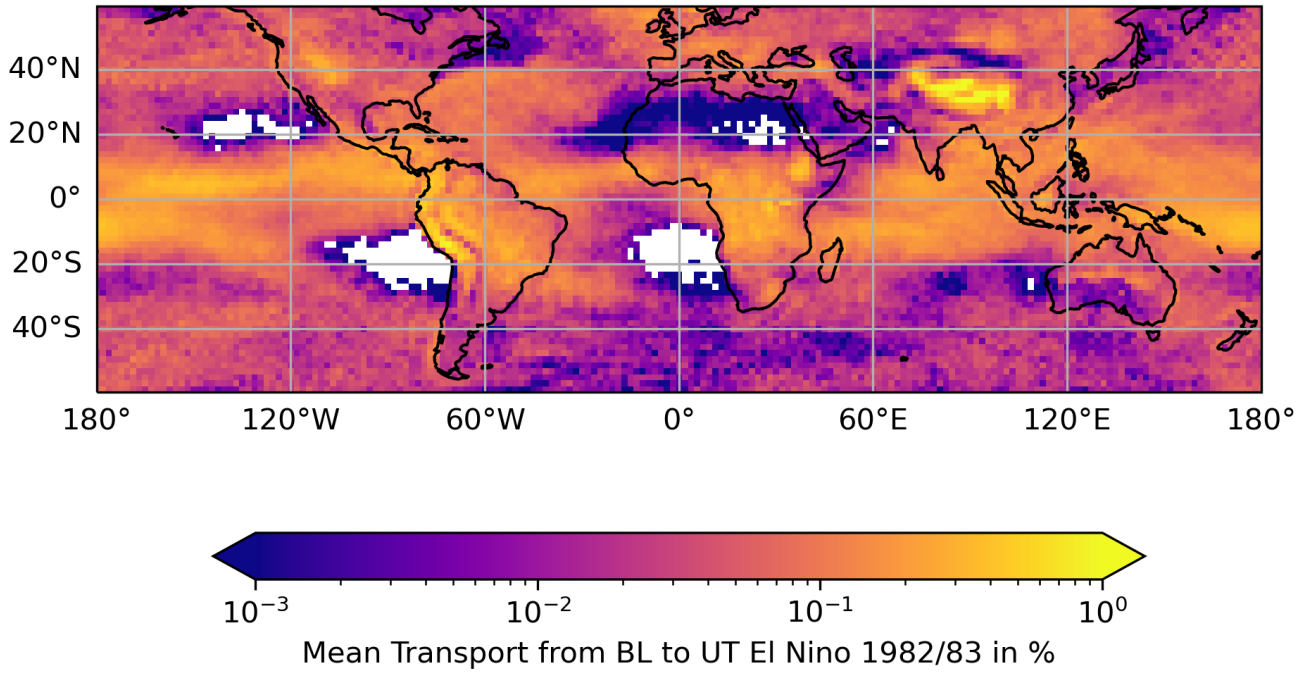

Figure S5: El Niño event 1982/83 convective mean transport from the planetary boundary layer height to upper troposphere within 12 min. The upper troposphere is defined as the region between the tropopause and the pressure height of tropopause plus 150 hPa.

References

S. Dietmüller, P. Jöckel, H. Tost, M. Kunze, C. Gellhorn, S. Brinkop, C. Frömming, M. Ponater, B. Steil, A. Lauer, and J. Hendricks. A new radiation infrastructure for the modular earth submodel system (messy, based on version 2.51). *Geoscientific Model Development*, 9(6):2209–2222, 2016. doi: 10.5194/gmd-9-2209-2016. URL https://gmd.copernicus.org/articles/9/2209/2016/.

R. Eichinger and P. Jöckel. The generic messy submodel tendency (v1.0) for process-based analyses in earth system models. *Geoscientific Model Development*, 7(4):1573–1582, 2014. doi: 10.5194/gmd-7-1573-2014. URL https://gmd.copernicus.org/articles/7/1573/2014/.

M. A. Giorgetta and L. Bengtsson. Potential role of the quasi-biennial oscillation in the stratosphere-troposphere exchange as found in water vapor in general circulation model experiments. *Journal of Geophysical Research: Atmospheres*, 104(D6):6003–6019, 1999. doi: https://doi.org/10.1029/1998JD200112. URL https://agupubs.onlinelibrary.wiley.com/doi/abs/10.1029/1998JD200112.

S. Hagemann. An improved land surface parameter dataset for global and regional climate models. 2002. Max-Planck-Institut für Meteorologie, Report No. 336.

P. Jöckel, R. Sander, A. Kerkweg, H. Tost, and J. Lelieveld. Technical note: The modular earth submodel system (messy) - a new approach towards earth system modeling. *Atmospheric Chemistry and Physics*, 5(2):433–444, 2005. doi: 10.5194/acp-5-433-2005. URL https://acp.copernicus.org/articles/5/433/2005/.

P. Jöckel, H. Tost, A. Pozzer, C. Brühl, J. Buchholz, L. Ganzeveld, P. Hoor, A. Kerkweg, M. G. Lawrence, R. Sander, B. Steil, G. Stiller, M. Tanarhte, D. Taraborrelli, J. van Aardenne, and J. Lelieveld. The atmospheric chemistry general circulation model echam5/messy1: consistent simulation of ozone from the surface to the mesosphere. *Atmospheric Chemistry and Physics*, 6(12):5067–5104, 2006. doi: 10.5194/acp-6-5067-2006. URL https://acp.copernicus.org/articles/6/5067/2006/.

P. Jöckel, A. Kerkweg, J. Buchholz-Dietsch, H. Tost, R. Sander, and A. Pozzer. Technical note: Coupling of chemical processes with the modular earth submodel system (messy) submodel tracer. *Atmospheric Chemistry and Physics*, 8(6):1677–1687, 2008. doi: 10.5194/acp-8-1677-2008. URL https://acp.copernicus.org/articles/8/1677/2008/.

P. Jöckel, A. Kerkweg, A. Pozzer, R. Sander, H. Tost, H. Riede, A. Baumgaertner, S. Gromov, and B. Kern. Development cycle 2 of the modular earth submodel system (messy2). *Geoscientific Model Development*, 3(2):717–752, 2010. doi: 10.5194/gmd-3-717-2010. URL https://gmd.copernicus.org/articles/3/717/2010/.

A. Kerkweg and P. Jöckel. The infrastructure messy submodels grid (v1.0) and import (v1.0). *Geoscientific Model Development Discussions*, 8:8607–8633, 2015. doi: 10.5194/gmdd-8-8607-2015. URL https://gmd.copernicus.org/preprints/8/8607/2015/.

A. Kerkweg, R. Sander, H. Tost, and P. Jöckel. Technical note: Implementation of prescribed (offlem), calculated (onlem), and pseudo-emissions (tnudge) of chemical species in the modular earth submodel system (messy). *Atmospheric Chemistry and Physics*, 6(11):3603–3609, 2006. doi: 10.5194/acp-6-3603-2006. URL https://acp.copernicus.org/articles/6/3603/2006/.

A. Kerkweg, C. Hofmann, P. Jöckel, M. Mertens, and G. Pante. The on-line coupled atmospheric chemistry model system meco(n) – part 5: Expanding the multi-model-driver (mmd v2.0) for 2-way data exchange including data interpolation via grid (v1.0). *Geoscientific Model Development*, 11(3):1059–1076, 2018. doi: 10.5194/gmd-11-1059-2018. URL https://gmd.copernicus.org/articles/11/1059/2018/.

J. Landgraf and P. J. Crutzen. An efficient method for online calculations of photolysis and heating rates. *Journal of the Atmospheric Sciences*, 55(5):863 – 878, 1998. doi: 10.1175/1520-0469(1998)055⟨0863:AEMFOC⟩2.0.CO;2. URL https://journals.ametsoc.org/view/journals/atsc/55/5/1520-0469_1998_055_0863_aemfoc_2.0.co_2.xml.

U. Lohmann and E. Roeckner. Design and performance of a new cloud microphysics scheme developed for the echam general circulation model. *Climate Dynamics*, 12:557–572, 1996. doi: 10.1007/BF00207939. URL https://doi.org/10.1007/BF00207939.

T.-E. Nordeng. Extended versions of the convective parametrization scheme at ecmwf and their impact on the mean and transient activity of the model in the tropics. *ECMWF Technical Memoranda*, (206):1–41, 09/1994 1994. doi: 10.21957/e34xwhysw. URL https://www.ecmwf.int/node/11393.

M. Nützel, L. Stecher, P. Jöckel, F. Winterstein, M. Dameris, M. Ponater, P. Graf, and M. Kunze. Updating the radiation infrastructure in messy (based on messy version 2.55). *Geoscientific Model Development*, 17(15):5821–5849, 2024. doi: 10.5194/gmd-17-5821-2024. URL https://gmd.copernicus.org/articles/17/5821/2024/.

H. G. Ouwersloot, A. Pozzer, B. Steil, H. Tost, and J. Lelieveld. Revision of the convective transport module cvtrans 2.4 in the emac atmospheric chemistry–climate model. *Geoscientific Model Development*, 8(8):2435–2445, 2015. doi: 10.5194/gmd-8-2435-2015. URL https://gmd.copernicus.org/articles/8/2435/2015/.

E. Roeckner, R. Brokopf, M. Esch, M. Giorgetta, S. Hagemann, L. Kornblueh, E. Manzini, U. Schlese, and U. Schulzweida. Sensitivity of simulated climate to horizontal and vertical resolution in the echam5 atmosphere model. *Journal of Climate*, 19(16):3771 – 3791, 2006. doi: 10.1175/JCLI3824.1. URL https://journals.ametsoc.org/view/journals/clim/19/16/jcli3824.1.xml.

R. Sander, P. Jöckel, O. Kirner, A. T. Kunert, J. Landgraf, and A. Pozzer. The photolysis module jval-14, compatible with the messy standard, and the jval preprocessor (jvpp). *Geoscientific Model Development*, 7(6):2653–2662, 2014. doi: 10.5194/gmd-7-2653-2014. URL https://gmd.copernicus.org/articles/7/2653/2014/.

M. Tiedtke. A comprehensive mass flux scheme for cumulus parameterization in large-scale models. *Monthly Weather Review*, 117(8):1779 – 1800, 1989. doi: 10.1175/1520-0493(1989)117⟨1779:ACMFSF⟩2.0.CO;2. URL https://journals.ametsoc.org/view/journals/mwre/117/8/1520-0493_1989_117_1779_acmfsf_2_0_co_2.xml.

H. Tost, P. Jöckel, and J. Lelieveld. Influence of different convection parameterisations in a gcm. *Atmospheric Chemistry and Physics*, 6(12):5475–5493, 2006. doi: 10.5194/acp-6-5475-2006. URL https://acp.copernicus.org/articles/6/5475/2006/.

H. Tost, M. G. Lawrence, C. Brühl, P. Jöckel, and The GABRIEL Team and The SCOUT-O3-DARWIN/ACTIVE Team. Uncertainties in atmospheric chemistry modelling due to convection parameterisations and subsequent scavenging. *Atmospheric Chemistry and Physics*, 10(4):1931–1951, 2010. doi: 10.5194/acp-10-1931-2010. URL https://acp.copernicus.org/articles/10/1931/2010/.

F. Winterstein and P. Jöckel. Methane chemistry in a nutshell – the new submodels ch4 (v1.0) and trsync (v1.0) in messy (v2.54.0). *Geoscientific Model Development*, 14(2):661–674, 2021. doi: 10.5194/gmd-14-661-2021. URL https://gmd.copernicus.org/articles/14/661/2021/.